Calculating the Characteristic Impedance of Finlines by Transverse Resonance Method

JENS BORNEMANN AND FRITZ ARNDT, SENIOR MEMBER, IEEE

Abstract —The characteristic impedance of finlines with up to three slots is calculated by a rigorous hybrid-mode analysis which includes the finite metallization thickness and finite depth of the mounting grooves. The transverse resonance principle utilized reduces considerably the order of the involved matrix eigenvalue problem. The propagation constants for the fundamental HE_1 mode (and EH_0 mode at related structures), as well as for the higher order modes (up to HE_7), and the characteristic impedances for the fundamental modes are computed as a function of frequency for the bilateral and unilateral finline, as well as for the unilateral finline with two coupled slots, and an additional slot on the opposite side of the substrate surface. The finite metallization thickness and mounting groove depth considered show significant influence on the behavior of the characteristic impedance.

I. Introduction

FINLINES ARE OF increasing importance for millimeter-wave integrated circuits. Extended application of such structures requires realistic design data including suitably defined characteristic impedances. Although effective hybrid-mode formulations for analyzing many configurations have been presented in the past, e.g., [1]–[6], real structure parameters, like finite metallization thickness and finite depth of the longitudinal grooves for mounting the substrate, have been taken into account only scarcely.

These parameters may considerably influence circuit behavior, especially for higher operating frequencies, as has been demonstrated, more recently, for the propagation constant of various types of finline configurations [7]–[9]. As for the characteristic impedance, the finite metallization thickness has hitherto been taken into account only for unilateral and bilateral finlines [10] utilizing the equivalent circuit concept in the spectral domain [3], and for unilateral finlines with grooves [7]. The decoupled TE–TM formulation in [7] is considered, however, to yield only approximate results.

In order to improve the flexibility of applying such millimeter-wave components, in this paper, the hybrid-mode transverse resonance method [11] is extended for calculating the characteristic impedance of more complex types of finlines (Fig. 1). As has already been shown with shielded microstrip lines [11], dielectric waveguides [12], and, more recently, with finlines, [8], [9], [13], the size of the characteristic matrix equation resulting from the transverse resonance condition is reduced considerably, e.g., compared with the usual mode-matching technique. Moreover, by simply modifying only a few coupling and transmission matrices, a variety of structures may be included. The finite metallization and mounting groove problem is taken into account in the theory. Comparison with available results in some special cases [2], [4], [10] establishes the accuracy of the numerical solutions.

Manuscript received March 1, 1985; revised July 18, 1985.

The authors are with the Microwave Department, University of Bremen, Kufsteiner Strasse, NW 1, D-2800 Bremen 33, West Germany.

IEEE Log Number 8405812.

II. Theory

A. Eigenvalue Problem

Since the derivation of the characteristic matrix equation of the finline structures in Fig. 1 has already been presented in [8] and [9], this part of the theory is given in only abbreviated form. For details, the reader is referred to [8] and [9].

The hybrid modes on the finline structures in Fig. 1 are derived from the z-components of the vector potentials $\vec{A}_h$ and $\vec{A}_e$

$$\vec{E} = \nabla \times \vec{A}_{hz} + \frac{1}{j\omega\epsilon} \nabla \times \nabla \times \vec{A}_{ez}$$

$$\vec{H} = \nabla \times \vec{A}_{ez} - \frac{1}{j\omega\mu} \nabla \times \nabla \times \vec{A}_{hz}. \tag{1}$$

A_{hz} and A_{ez} are assumed to be a sum of suitable eigenmodes in each subregion

$$A^{\nu}_{h,ez} = V^{\nu}_{h,e}(x,y) e^{-jk_z z} \tag{2}$$

where

$$V_h(x,y) = \sum_{n=0}^{N} Q_{hn}(x) f_n(y)$$

$$V_e(x,y) = \sum_{n=0}^{N} P_{en}(x) g_n(y) \tag{3a}$$

with

$$f_n(y) = \frac{\cos(k_y \tilde{y})}{\sqrt{1+\delta_{on}}} \tag{3b}$$

$$g_n(y) = \sin(k_y \tilde{y}), \qquad \delta_{on} = \text{Kronecker delta}. \tag{3c}$$

$k_y \tilde{y}$ corresponds to the y-dependent boundary condition in each subregion ($\nu \in$ I, II, III, IV, V, cf. Fig. 1(a)) or ($\nu \in$ I, II, III, IVa, IVb, V, cf. Fig. 1(b)), respectively, as follows:

$$k^{\nu}_y \tilde{y}^{\nu} = \frac{n\pi}{f^{\nu}} \cdot q^{\nu} \tag{4}$$

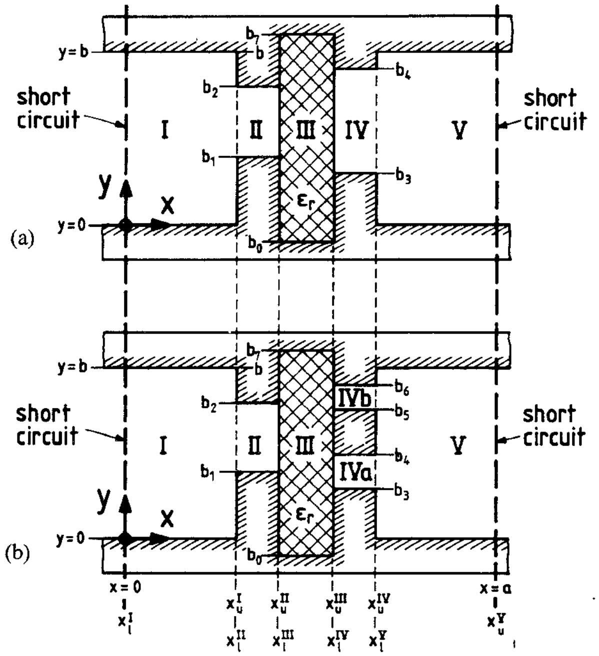

Fig. 1. Finline structures including finite-metallization thickness and mounting groove depth. (a) Bilateral finline. (b) Finline with two coupled slots and a slot on the opposite side of the substrate.

where f^ν and q^ν for Fig. 1(a) are given by

$$f^\nu = [b, b_2 - b_1, b_7 - b_0, b_4 - b_3, b]$$
$$q^\nu = [y, y - b_1, y - b_0, y - b_3, y] \tag{5a}$$

and for Fig. 1(b)

$$f^\nu = [b, b_2 - b_1, b_7 - b_0, b_4 - b_3, b_6 - b_5, b]$$
$$q^\nu = [y, y - b_1, y - b_0, y - b_3, y - b_5, y] \tag{5b}$$

respectively.

The eigenfunctions $Q_h(x), P_e(x)$ in (3) can advantageously be regarded as representing waves traveling in the $\pm x$-direction, with the still unknown propagation constants k_x^ν in each subregion. The boundary conditions at the upper (x_u^ν) and lower (x_l^ν) boundary at the partial waveguides thus formed in the x-direction, successively applied for the transversal field components

$$E_y \alpha \frac{dQ_h}{dx} = P_h, E_z \alpha P_e, H_z \alpha Q_h, H_y \alpha \frac{dP_e}{dx} = Q_e \tag{6}$$

at each discontinuity, lead finally to the relation between the wave amplitudes at $x = 0$ and $x = a$ (Fig. 1)

$$\begin{bmatrix} P_h^{\mathrm{I}} \\ P_e^{\mathrm{I}} \\ Q_h^{\mathrm{I}} \\ Q_e^{\mathrm{I}} \end{bmatrix}_{x=0} = \underbrace{T^{\mathrm{I}} \cdot C^{\mathrm{I,II}} \cdot T^{\mathrm{II}} \cdot C^{\mathrm{II,III}} \cdot T^{\mathrm{III}} \cdot C^{\mathrm{III,IV}} \cdot T^{\mathrm{IV}} \cdot C^{\mathrm{IV,V}} \cdot T^{\mathrm{V}}}_{M} \cdot \begin{bmatrix} P_h^{\mathrm{V}} \\ P_e^{\mathrm{V}} \\ Q_h^{\mathrm{V}} \\ Q_e^{\mathrm{V}} \end{bmatrix}_{x=a} . \tag{7}$$

The transmission matrices T^ν transform the amplitudes from the upper (x_u^ν) to the lower (x_l^ν) boundary in each subregion ν, i.e., partial waveguide ν. The coupling matrices $C^{\nu,\nu+1}$ match the amplitudes at each discontinuity between adjacent partial waveguides $\nu, \nu+1$ in the x-direction. The related expressions for T and C are given in [8] and [9] and are reproduced in the Appendix using the present notation. Note that for replacing the finline structure of Fig. 1(a) by Fig. 1(b) only the transmission matrix T^{IV} and the coupling matrices $C^{\mathrm{III,IV}}$, $C^{\mathrm{IV,V}}$ need to be appropriately altered. A second advantage of this method is that the matrix size of M in (7) is constant, even for an increasing additional number of discontinuities, e.g., layered dielectric or additional grooves, since all matching steps are represented by coupling matrices in the matrix product of (7). Moreover, appropriate electric- and magnetic-wall symmetry conditions [8], [9] yield a further variety of, for instance, coupled structures.

The electric-wall boundary condition at $x = 0$ and $x = a$ ($E_z = E_y = 0$, i.e., $P_e = P_h = 0$, cf. (6) and (7)) leads to the transverse resonance condition

$$\begin{bmatrix} 0 \\ 0 \end{bmatrix} = \begin{bmatrix} M_{hh}^{12} & M_{he}^{12} \\ M_{eh}^{12} & M_{ee}^{12} \end{bmatrix} \begin{bmatrix} Q_h^V \\ Q_e^V \end{bmatrix} \tag{8}$$

where M^{12} is only the upper right quarter of the matrix M in (7). This reduction of matrix size is a further advantage of this method.The zeros of the determinant

$$\det(M^{12}) = 0 \tag{9}$$

which is a transcendent function of

$$k_{xn}^{\nu 2} = \epsilon_r^\nu k_0^2 - \left(\frac{n\pi}{f^\nu}\right)^2 - k_z^2 \tag{10}$$

with

$$k_0^2 = \omega^2 \mu_0 \epsilon_0$$

provide the desired frequency-dependent propagation constant k_z for the hybrid modes.

The transverse resonance method applied in the form of (7) and (8) requires an identical number of modes N (cf. (3a)) in each subregion, i.e., for example, $N = N^{\mathrm{I}} = N^{\mathrm{II}} = N^{\mathrm{III}} = N^{\mathrm{IVa}} + N^{\mathrm{IVb}} = N^{\mathrm{V}}$ for the structure of Fig. 1(b). Therefore, a further reduction of the number of equations is not possible by manipulating the system so that the unknowns are the wave amplitudes in the slot region, as, e.g., in [16].

B. Characteristic Impedance

To restrict the arbitrariness which is inherent to a certain extent to definitions of characteristic impedances for hybrid waveguiding structures [11], [14], [15], the utility for an appropriate lumped-circuit design [14] may be chosen as the basic criterion. A definition based on the power P transported along the finline is considered to promise such usefulness for design purposes. For the second sufficiently lumped quantity necessary for the definition of the characteristic impedance Z_0, the slot voltage U_r is chosen [1]–[4], [14]

$$Z_{0r} = \frac{U_r^2}{2P}. \tag{11}$$

The slot voltage of the rth slot can be found directly by integrating the corresponding slot field in the middle of the slot r

$$U_r = \int_{y_l^r}^{y_u^r} E_y^r\left(x = \frac{x_u^r - x_l^r}{2}, z = 0\right) dy \tag{12}$$

where x_u, x_l, y_u, y_l are the upper and lower boundaries in the x, y-directions, $\nu = \text{II, IV}$, (Fig. 1(a)), or II, IVa, IVb, (Fig. 1(b)), respectively. Equations (11), and (12) imply that for structures with several slots, different characteristic impedances may be defined. In this paper we consider only the slot with the minimum width (i.e., highest expected field concentration); for symmetrical structures, only one half is calculated utilizing electric-wall or magnetic-wall symmetry, respectively.

For an efficient inclusion of the mutual coupling effects of hybrid modes which may occur at finlines of complex structure, [8], [9], instead of the power associated with the rth slot [3]–[4], [14], the total average power P of the finline [2], [10] is chosen for calculating the characteristic impedance (11)

$$P = \frac{1}{2}\,\mathrm{Re}\left\{\sum_{\nu=I}^{V} \int_{F^\nu} (\vec{E}^\nu \times \vec{H}^{*\nu})\, d\vec{F}\right\} \tag{13}$$

where F^ν is the area of the νth subregion. The total power transported along the structure is considered to be sufficiently localized, but, on the other side, to be a suitable indication of a possible change in the field concentration due to mutual coupling effects.

The transverse components of the electromagnetic field, in each subregion, for the derivation of the related expressions for power and slot voltage, are calculated by (1)–(3), where P_{en}, Q_{hn} are given iteratively by

$$\begin{bmatrix} \boldsymbol{P}_h^{i-1}(x = x_u^{i-1}) \\ \boldsymbol{P}_e^{i-1}(x = x_u^{i-1}) \\ \boldsymbol{Q}_h^{i-1}(x = x_u^{i-1}) \\ \boldsymbol{Q}_e^{i-1}(x = x_u^{i-1}) \end{bmatrix}_{i = \text{II,III,IV,V}} = \boldsymbol{C}^{i-1,i} \cdot \boldsymbol{T}^i \begin{bmatrix} \boldsymbol{P}_h^i(x = x_u^i) \\ \boldsymbol{P}_e^i(x = x_u^i) \\ \boldsymbol{Q}_h^i(x = x_u^i) \\ \boldsymbol{Q}_e^i(x = x_u^i) \end{bmatrix}. \tag{14}$$

The values for $\boldsymbol{Q}_h^V(x = x_u^V = a), \boldsymbol{Q}_e^V(x = x_u^V = a)$ are calculated by solving the homogeneous matrix equation (8) substituting the propagation constant k_z given by (9) and (10); note that $\boldsymbol{P}_h^V(x = x_u^V = a) = \boldsymbol{P}_e^V(x = x_u^V = a) = \boldsymbol{0}$.

For the calculations, the expansion in 18 eigenmodes has turned out to yield sufficient asymptotic behavior of the curves presented in this paper. For the EH_0-mode operation of the finline structures in Fig. 1(b), a definition of the characteristic impedance via strip current I and power [4], [14] has also been applied, showing nearly identical results but requiring an increased number of modes to be considered (about 45).

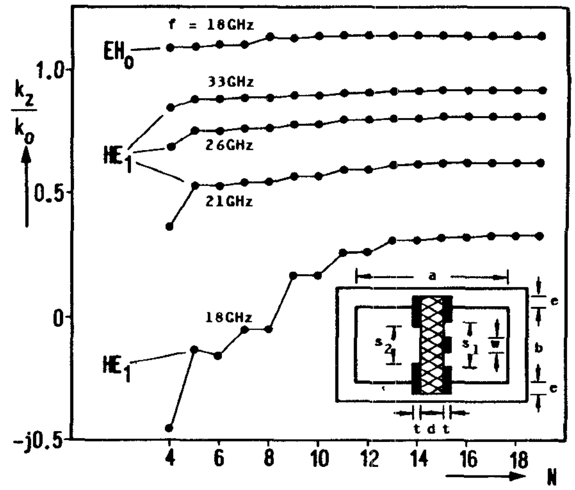

Fig. 2. Normalized propagation constant k_z/k_0 (k_0 = free-space wavenumber) as a function of the number N of eigenmodes (cf. (3a)) in each subregion, at different frequencies for a bilateral finline with two coupled slots on upper substrate side and one slot opposite; $a = 2b = 7.112$ mm, $d = 254$ μm, $t = 17.5$ μm, $w = b/5$, $s_1 = 3b/5$, $s_2 = b/2$, $e = 0.5$ mm, $\epsilon_r = 2.22$.

III. Results

Numerical aspects of the method are illustrated by the normalized propagation constant k_z/k_0 of the relatively complicated finline structure of Fig. 2 (bilateral finline with two coupled slots on the upper substrate surface and one slot on opposite side). It may be stated that the expansion in $N = 18$ eigenmodes in each subregion yield sufficient asymptotic behavior. Similar convergence behavior was stated for other structures, other frequencies, and for the calculation of the characteristic impedances by (11). Low relative convergence phenomena have been observed between about $N = 7 \cdots 14$.

For the bilateral finline, dispersion characteristics and the characteristic impedance of the fundamental HE_1 mode are shown in Fig. 3. The same dimensions as used by Schmidt and Itoh [2] are chosen (dashed lines), with the exception that a finite metallization thickness $t = 5$ μm is taken into account. Additionally, the effect of a finite groove depth $e = 0.35$ mm is considered for the practically important HE_1 and HE_7 modes (solid line), which are excited at symmetrical bilateral finline structures by a TE_{10} wave incident on the corresponding empty waveguide, and which define the actually relevant monomode range. The influence of groove depth on the higher order HE_2 and HE_3 modes (not excited by an incident TE_{10} wave) has already been discussed in [8].

The results in Fig. 3 are in good agreement with those available in [2]. The slight deviations in propagation constants and Z_0 values are due to the influence of the finite-metallization thickness considered, which reduces slightly the field concentration within the dielectric substrate in favor of the field within the two slots. As may be

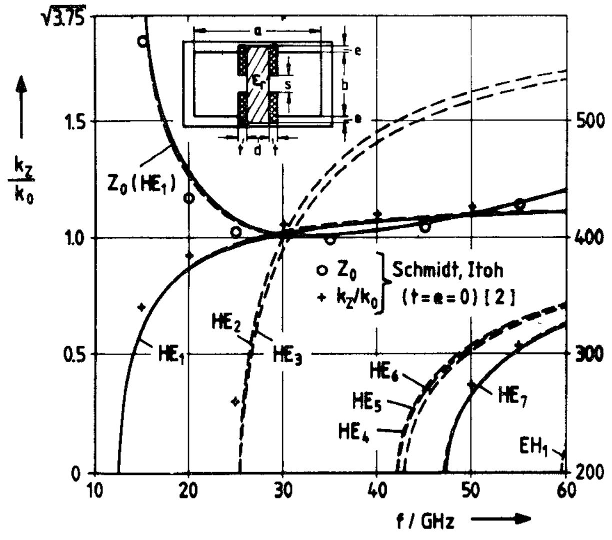

Fig. 3. Normalized propagation constant k_z/k_0 (k_0 = free-space wavenumber) and characteristic impedance Z_0 as a function of frequency for the bilateral finline. Metallization thickness: $t = 5$ μm. Groove depth: $e = 0$---- (dashed lines), $e = 0.35$ mm——(solid lines). Other parameters: $a = 2b = 7.112$ mm, $d = 125$ μm, $s = 0.5$ mm, $\epsilon_r = 3.75$

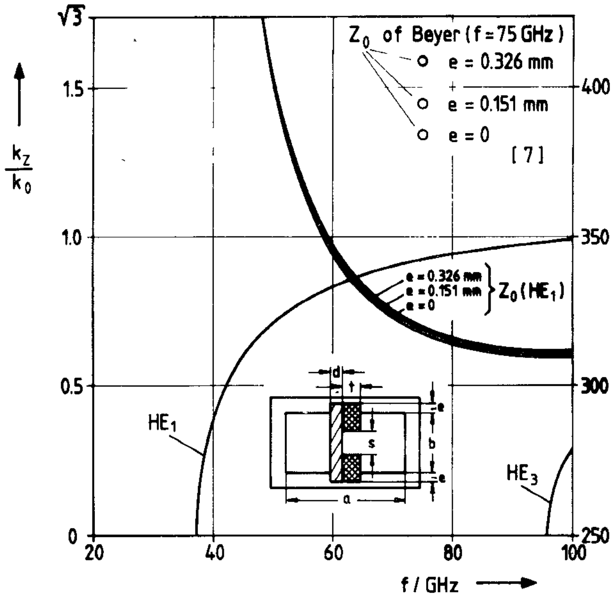

(a)

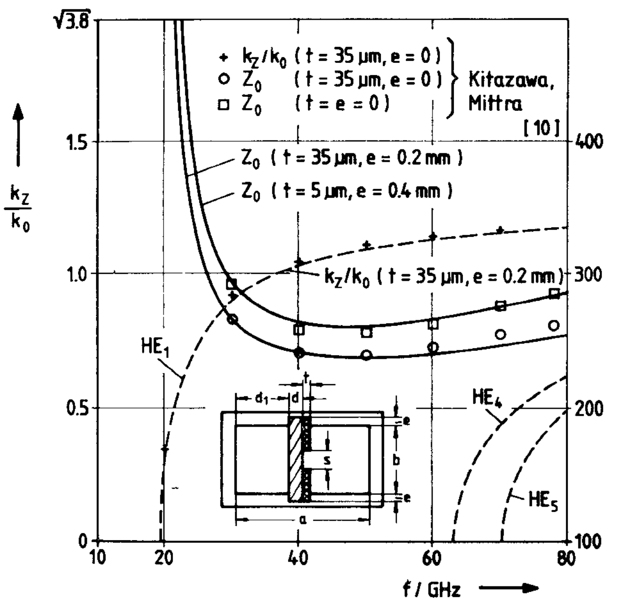

(b)

Fig. 4. Normalized propagation constant k_z/k_0 and characteristic impedance Z_0 as a function of frequency for the unilateral finline. (a) Dimensions according to Beyer [7]: $a = 2b = 3.1$ mm, $d = 50$ μm, $t = 70$ μm, $s = 0.6$ mm, $e = 0.326$ mm, $\epsilon_r = 3.0$. (b) Dimensions according to Kitazawa and Mittra [10], but with finite groove depth included

$$\left.\begin{array}{l} e = 0.2 \text{ mm} \\ t = 35\ \mu\text{m} \end{array}\right\} \text{---- (dashed lines)}$$

$$\left.\begin{array}{l} e = 0.4 \text{ mm} \\ t = 5\ \mu\text{m} \end{array}\right\} \text{—— (solid lines)}$$

$a = 2b = 4.7752$ mm, $d_1 = 2.2606$ mm, $d = 127$ μm, $s = 0.1a$, $\epsilon_r = 3.8$.

stated by comparing the corresponding solid with the dashed curves, the influence of the mounting groove depth e on the HE_1- and HE_7-mode dispersion and characteristic impedance behavior is negligible for the symmetric bilateral finline, since relevant HE_1- and HE_7- field parameters, e.g., the cutoff frequencies, are influenced only moderately by the groove depth e [8].

Unilateral finline examples are presented in Figs. 4 and 5. The structure treated by Beyer [7] is calculated with our method. The results (Fig. 4(a)) do not agree with those available in [7]. In Fig. 4(b), the same dimensions as those used by Kitazawa and Mittra [10] are chosen, with the exception that a finite groove depth $e = 0.2$ mm (for $t = 35$ μm), and $e = 0.4$ mm (for $t = 5$ μm) is taken into account. The results are in good agreement with those of [10]. The slight deviation of Z_0 for $t = 35$ μm at higher frequencies is due to the change in the field concentration caused by the finite groove depth taken into account. The slightly higher characteristic impedance values for $t = 5$ μm, compared with $t = 0$ of [10], is attributable to the increase of the electric field between the slots caused by the finite-metallization thickness considered. The severe influence of waveguide groove depth at unilateral finlines with the usual substrate thicknesses is demonstrated in Fig. 5. Finite groove depth (solid line) leads to decreasing higher order mode cutoff frequencies which cause significant deviations in propagation constant and characteristic impedance behavior. The fundamental HE_1-mode characteristic impedance $Z_0(HE_1)$ decreases significantly for higher frequencies. This effect is brought about by the higher order HE_3 mode, which is propagative already at about 60 GHz and causes an increasing field concentration within the dielectric substrate (cf. the increase of the corresponding propagation constant).

Similar behavior is observed for unilateral finlines with two coupled slots as shown in Fig. 6. As long as the groove depth is neglected (Fig. 6(a)), the calculated dispersion and characteristic impedance characteristics, for the two fundamental EH_0 and HE_1 modes on this structure excited by an incident TE_{01}- and TE_{10}-waveguide wave, respectively, agree well with investigations by Schmidt [4]. Considering a finite groove depth (Fig. 6(b)), however, the monomode

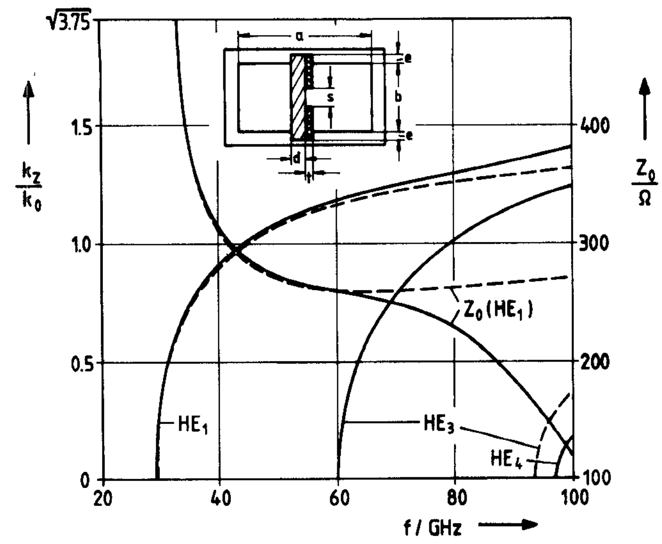

Fig. 5. Normalized propagation constant k_z/k_0 and characteristic impedance Z_0 as a function of frequency for the unilateral finline. Metallization thickness: $t = 5$ μm, $a = 2b = 3.1$ mm, $d = 220$ μm, $s = 0.4$ mm, $\epsilon_r = 3.75$. ——— (solid line) $e = 0.5$ mm, ---- (dashed line) $e = 0$.

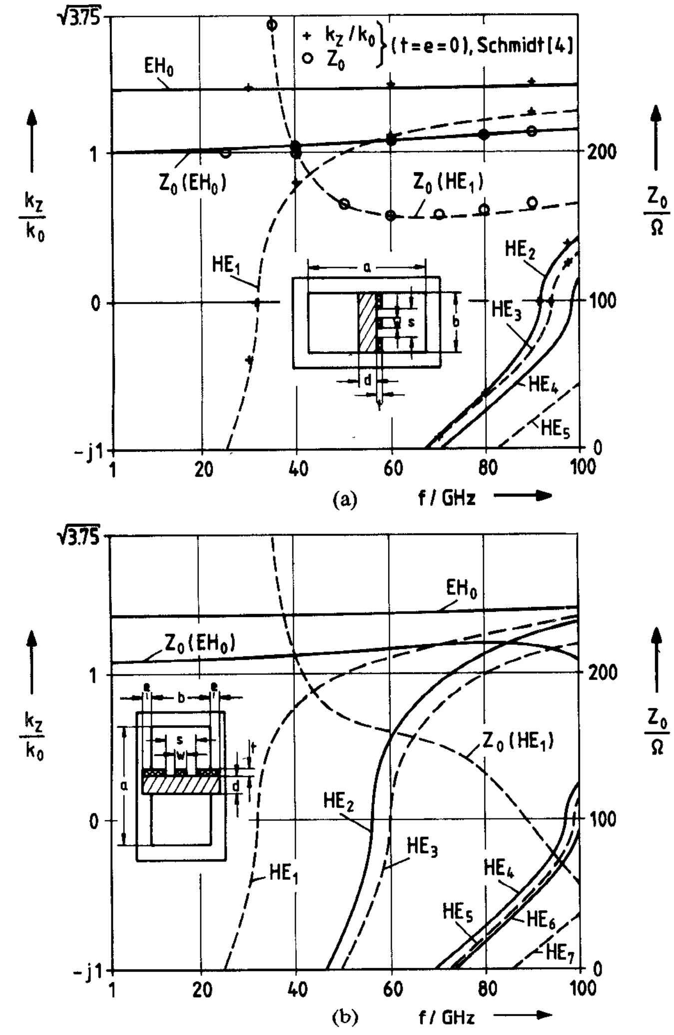

Fig. 6. Normalized propagation constant k_z/k_0 and characteristic impedance Z_0 as a function of frequency for the unilateral finline with two coupled slots. Metallization thickness: $t = 5$ μm, $a = 2b = 3.1$ mm, $d = 220$ μm, $w = 0.2$ mm, $s = 0.6$ mm, $\epsilon_r = 3.75$. ——— (solid line) magnetic-wall field symmetry at $y = b/2$. ---- (dashed line) electric-wall field symmetry at $y = b/2$. (a) Groove depth $e = 0$. (b) Groove depth $e = 0.5$ mm.

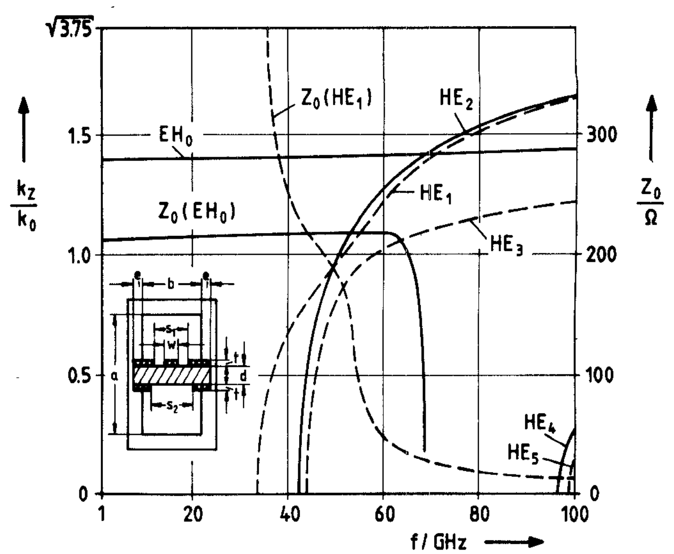

Fig. 7. Normalized propagation constant k_z/k_0 and characteristic impedance Z_0 as a function of frequency for the finline with two coupled slots and a slot on opposite substrate side. Metallization thickness: $t = 5$ μm. Groove depth: $e = 0.5$ mm. Other parameters: $a = 2b = 3.1$ mm, $d = 220$ μm, $w = 0.2$ mm, $s_1 = 0.7$ mm, $s_2 = 0.9$ mm, $\epsilon_r = 3.75$. ——— (solid lines) magnetic-wall field symmetry at $y = b/2$. ---- (dashed line) electric-wall field symmetry at $y = b/2$.

application ranges of both the EH_0 and HE_1 fundamental modes are reduced by the higher order HE_2 and HE_3 modes, respectively. The characteristic impedance $Z_0(EH_0)$ of the EH_0 mode is higher because the finite groove depth assists the progress of an odd E_y field within the slots; the growing field concentration within the dielectric caused by the HE_2 mode at higher frequencies, however, compensates this effect.

A slot on the opposite substrate surface (Fig. 7) increases the mutual higher order mode coupling effects caused by the finite groove depth, significantly. At about 50 GHz, and especially at about 70 GHz, an abrupt increasing field concentration within the dielectric substrate, initiated by the finite groove depth, distorts both dispersion and characteristic impedance behavior at these frequencies.

The theory given in this paper may be verified experimentally by the investigation of a structure similar to Fig. 7 but with two coupled strips, instead of the slots, on the upper side of the substrate. Suitable choice of the slot width s_2 on the lower substrate surface equalizes the velocities of the even and odd quasi-TEM modes [4] and so improves the directivity of related contra-directional couplers. The optimum slot width $s_{2\mathrm{opt}}$ was calculated [17] using the transverse resonance technique, and the results agree well with measured data published in [18].

IV. Conclusion

The rigorous hybrid-mode analysis described for calculating the characteristic impedance of finlines takes the finite-metallization thickness and finite depth of the substrate mounting grooves into account. The numerical examples given for the bilateral and unilateral finline, as well as for the unilateral finline with two coupled slots, and an additional slot on the opposite side of the substrate surface, demonstrate that the inclusion of these real structure parameters may be important for finline designs, especially for higher operating frequencies. Besides the considerable reduction of the matrix size of the involved eigenvalue problem, the transverse resonance method utilized has the advantage that the characteristic impedance of a great variety of relatively complex finline structures may be calculated by merely modifying appropriate coupling and transmission matrices, and by including suitable electric- and magnetic-wall symmetry, within the corresponding matrix equation. Comparison with available results for some special examples of the spectral-domain method, for zero groove depth, as well as for zero and finite-metallization thickness, shows good agreement.

Appendix

Transmission Matrices T^ν in (7)

Finline Type in Fig. 1(a):

$$\boldsymbol{T}^\nu = \begin{bmatrix} \boldsymbol{T}_c^\nu & \mathbf{0} & \boldsymbol{T}_{cs}^\nu & \mathbf{0} \\ \mathbf{0} & \boldsymbol{T}_c^\nu & \mathbf{0} & \boldsymbol{T}_s^\nu \\ \boldsymbol{T}_s^\nu & \mathbf{0} & \boldsymbol{T}_c^\nu & \mathbf{0} \\ \mathbf{0} & \boldsymbol{T}_{cs}^\nu & \mathbf{0} & \boldsymbol{T}_c^\nu \end{bmatrix}, \qquad \nu = \mathrm{I}, \mathrm{II}, \cdots, \mathrm{V} \quad \text{(A1)}$$

with

$$\boldsymbol{T}_c^\nu = \operatorname{diag}\{\cos(k_{xn}^\nu d^\nu)\}$$
$$\boldsymbol{T}_{cs}^\nu = \operatorname{diag}\{-k_{xn}^\nu \cdot \sin(k_{xn}^\nu d^\nu)\}$$
$$\boldsymbol{T}_s^\nu = \operatorname{diag}\left\{\frac{1}{k_{xn}^\nu}\sin(k_{xn}^\nu d^\nu)\right\} \qquad \text{(A2)}$$

where $d^\nu = x_l^\nu - x_u^\nu$, and diag is a diagonal matrix.

Finline Type in Fig. 1(b):

Merely $\boldsymbol{T}_c^{\mathrm{IV}}$, $\boldsymbol{T}_{cs}^{\mathrm{IV}}$, and $\boldsymbol{T}_s^{\mathrm{IV}}$ in $\boldsymbol{T}^{\mathrm{IV}}$ of (A1) and (A2) need to be replaced by the corresponding submatrices

$$\begin{pmatrix} \boldsymbol{T}_c^{\mathrm{IVa}} & \mathbf{0} \\ \mathbf{0} & \boldsymbol{T}_c^{\mathrm{IVb}} \end{pmatrix} \text{etc.}$$

of identical rank, with k_{xn}^{IVa} and k_{xn}^{IVb}, respectively.

Coupling matrices $\boldsymbol{C}^{\nu,\nu+1}$ in (7)

Finline Type in Fig. 1(a):

$$\boldsymbol{C}^{\mathrm{I,II}} = \begin{bmatrix} \frac{2}{b}\boldsymbol{J}_c^{I,II} & \mathbf{0} & \mathbf{0} & \mathbf{0} \\ \mathbf{0} & \frac{2}{b}\boldsymbol{J}_s^{\mathrm{I,II}} & \mathbf{0} & \mathbf{0} \\ \mathbf{0} & \mathbf{0} & \frac{b_2-b_1}{2}\left[(\boldsymbol{J}_c^{\mathrm{I,II}})^{\mathrm{tr}}\right]^{-1} & \mathbf{0} \\ \mathbf{0} & \mathbf{0} & \mathbf{0} & \frac{b_2-b_1}{2}\left[(\boldsymbol{J}_s^{\mathrm{I,II}})^{\mathrm{tr}}\right]^{-1} \end{bmatrix} \qquad \text{(A3)}$$

with the coupling integrals

$$J_{cnk}^{\nu,\xi} = \int_{b_l^\nu}^{b_u^\nu} f_n^\nu(y) f_k^\xi(y)\, dy \qquad \text{(A4)}$$

and where tr means transposed.

For J_s, replace $f_{n,k}(y)$ by $g_{n,k}(y)$ (cf. (3b) and (3c)); $\nu, \xi \in (\mathrm{I,II,III,IV,V})$; b_l^ν, b_u^ν, lower and upper y boundary within the subregion ν

$$\boldsymbol{C}^{\mathrm{II,III}} = \begin{bmatrix} \frac{b_7-b_0}{2}\left[(\boldsymbol{J}_c^{\mathrm{II,III}})^{\mathrm{tr}}\right]^{-1} & e_5\left[(\boldsymbol{J}_c^{\mathrm{II,III}})^{\mathrm{tr}}\right]^{-1}\boldsymbol{D}^n & \mathbf{0} & \mathbf{0} \\ \mathbf{0} & \frac{b_7-b_0}{2e_2}\left[(\boldsymbol{J}_s^{\mathrm{II,III}})\right]^{\mathrm{tr}}]^{-1} & \mathbf{0} & \mathbf{0} \\ \mathbf{0} & \mathbf{0} & \frac{2e_3}{b_2-b_1}\boldsymbol{J}_c^{\mathrm{II,III}} & \mathbf{0} \\ \mathbf{0} & \mathbf{0} & \frac{-2e_4}{b_2-b_1}\boldsymbol{J}_s^{\mathrm{II,III}}\boldsymbol{D}^{\mathrm{III}} & \frac{2}{b_2-b_1}\boldsymbol{J}_s^{\mathrm{II,III}} \end{bmatrix} \qquad \text{(A5)}$$

with

$$e_5 = \frac{k_z}{\omega\epsilon_0}\frac{1/\epsilon_r - 1}{1-k_{z0}^2} \qquad e_2 = \epsilon_r \frac{1-k_{z0}^2}{\epsilon_r - k_{z0}^2}$$

$$e_4 = \frac{k_z}{\omega\mu_0}\frac{\epsilon_r - 1}{1-k_{z0}^2} \qquad k_{z0} = k_z/k_0 \text{ (normalized propagation constant)}$$

$$D^n = \operatorname{diag}\left(\frac{n\pi}{2}\right) \quad D^{\mathrm{III}} = \operatorname{diag}\left(\frac{n\pi}{b_7 - b_0}\right)$$

$$C^{\mathrm{III,IV}} = \begin{bmatrix} \frac{2}{b_7-b_0} J_c^{\mathrm{III,IV}} & \frac{2}{b_7-b_0} e_6 J_c^{\mathrm{III,IV}} D^{\mathrm{IV}} & \mathbf{0} & \mathbf{0} \\ \mathbf{0} & \frac{2}{b_7-b_0} e_2 J_s^{\mathrm{III,IV}} & \mathbf{0} & \mathbf{0} \\ \mathbf{0} & \mathbf{0} & \frac{b_4-b_3}{2\epsilon_r} e_2 \left[\left(J_c^{\mathrm{III,IV}}\right)^{\mathrm{tr}}\right]^{-1} & \mathbf{0} \\ \mathbf{0} & \mathbf{0} & e_7 \left[\left(J_s^{\mathrm{III,IV}}\right)^{\mathrm{tr}}\right]^{-1} D^k & \frac{b_4-b_3}{2}\left[\left(J_s^{\mathrm{III,IV}}\right)^{\mathrm{tr}}\right]^{-1} \end{bmatrix} \tag{A6}$$

with

$$e_6 = \frac{k_z}{\omega\epsilon_0}\frac{\epsilon_r - 1}{\epsilon_r - k_{z0}^2} \qquad e_7 = \frac{k_z}{\omega\mu_0}\frac{\epsilon_r - 1}{\epsilon_r - k_{z0}^2}$$

$$D^{\mathrm{IV}} = \operatorname{diag}\left(\frac{k\pi}{b_4 - b_3}\right) \quad D^k = \operatorname{diag}\left(\frac{k\pi}{2}\right)$$

$$C^{\mathrm{V,V}} = \begin{bmatrix} \frac{b}{2}\left(J_c^{\mathrm{V,IV}}\right)^{-1} & \mathbf{0} & \mathbf{0} & \mathbf{0} \\ \mathbf{0} & \frac{b}{2}\left(J_s^{\mathrm{V,IV}}\right)^{-1} & \mathbf{0} & \mathbf{0} \\ \mathbf{0} & \mathbf{0} & \frac{2}{b_4-b_3}\left(J_c^{\mathrm{V,IV}}\right)^{\mathrm{tr}} & \mathbf{0} \\ \mathbf{0} & \mathbf{0} & \mathbf{0} & \frac{2}{b_4-b_3}\left(J_s^{\mathrm{V,IV}}\right)^{\mathrm{tr}} \end{bmatrix} \tag{A7}$$

with the coupling integrals (ξ of higher order than ν)

$$J_{cnk}^{\xi,\nu} = \int_{b_l^\nu}^{b_u^\nu} f_n^\xi(y) f_k^\nu(y)\, dy. \tag{A8}$$

For J_s, again replace $f_{n,k}$ by $g_{n,k}$ (cf. (A4)).

For the finline type in Fig. 1(b), the coupling matrices $C^{\mathrm{III,IV}}$ and $C^{\mathrm{IV,V}}$ are replaced by

$$C^{\mathrm{III,IV}} = \begin{bmatrix} E^{\mathrm{III,IV}} & \mathbf{0} \\ \mathbf{0} & \left(H^{\mathrm{III,IV}}\right)^{-1} \end{bmatrix}$$

$$C^{\mathrm{IV,V}} = \begin{bmatrix} \left(E^{\mathrm{IV,V}}\right)^{-1} & \mathbf{0} \\ \mathbf{0} & H^{\mathrm{IV,V}} \end{bmatrix} \tag{A9}$$

where

$$E^{\mathrm{III,IV}} = \frac{2}{b_7 - b_0} \cdot \begin{bmatrix} J_c^{\mathrm{III,IVa}} & J_c^{\mathrm{III,IVb}} & e_1 J_c^{\mathrm{III,IVa}} D^{\mathrm{IVa}} & e_1 J_c^{\mathrm{III,IVb}} D^{\mathrm{IVb}} \\ \mathbf{0} & \mathbf{0} & e_2 J_s^{\mathrm{III,IVa}} & e_2 J_s^{\mathrm{III,IVb}} \end{bmatrix}$$

with

$$e_1 = \frac{k_z}{\omega\epsilon_0}\frac{1}{\epsilon_r - k_{z0}^2} \qquad D^{\mathrm{IVa}} = \operatorname{diag}\left(\frac{n\pi}{b_4 - b_3}\right)$$

$$D^{\mathrm{IVb}} = \operatorname{diag}\left(\frac{n\pi}{b_6 - b_5}\right)$$

$$E^{\mathrm{IV,V}} = \frac{b}{2}\begin{bmatrix} J_c^{\mathrm{V,IVa}} & J_c^{\mathrm{V,IVb}} & \mathbf{0} & \mathbf{0} \\ \mathbf{0} & \mathbf{0} & J_s^{\mathrm{V,IVa}} & J_s^{\mathrm{V,IVb}} \end{bmatrix}$$

and

$$\boldsymbol{H}^{\mathrm{III,IV}} = \begin{bmatrix} \frac{2e_3}{b_4-b_3}\left(\boldsymbol{J}_c^{\mathrm{III,IVa}}\right)^{\mathrm{tr}} & \boldsymbol{0} \\ \frac{2e_3}{b_6-b_5}\left(\boldsymbol{J}_c^{\mathrm{III,IVb}}\right)^{\mathrm{tr}} & \boldsymbol{0} \\ \frac{-2e_4}{b_4-b_3}\left(\boldsymbol{J}_s^{\mathrm{III,IVa}}\right)^{\mathrm{tr}}\boldsymbol{D}^{\mathrm{III}} & \frac{2}{b_4-b_3}\left(\boldsymbol{J}_s^{\mathrm{III,IVa}}\right)^{\mathrm{tr}} \\ \frac{-2e_4}{b_6-b_5}\left(\boldsymbol{J}_s^{\mathrm{III,IVb}}\right)^{\mathrm{tr}}\boldsymbol{D}^{\mathrm{III}} & \frac{2}{b_6-b_5}\left(\boldsymbol{J}_s^{\mathrm{III,IVb}}\right)^{\mathrm{tr}} \end{bmatrix} \tag{A10}$$

with

$$e_3 = \frac{\epsilon_r - k_{z0}^2}{1-k_{z0}^2}$$

$$\boldsymbol{H}^{\mathrm{IV,V}} = \begin{bmatrix} \frac{b_4-b_3}{2}\left(\boldsymbol{J}_c^{\mathrm{V,IVa}}\right)^{\mathrm{tr}} & \boldsymbol{0} \\ \frac{b_6-b_5}{2}\left(\boldsymbol{J}_c^{\mathrm{V,IVb}}\right)^{\mathrm{tr}} & \boldsymbol{0} \\ \boldsymbol{0} & \frac{b_4-b_3}{2}\left(\boldsymbol{J}_s^{\mathrm{V,IVa}}\right)^{\mathrm{tr}} \\ \boldsymbol{0} & \frac{b_6-b_5}{2}\left(\boldsymbol{J}_s^{\mathrm{V,IVb}}\right)^{\mathrm{tr}} \end{bmatrix}. \tag{A11}$$

For the coupling integrals (A4) and (A8), respectively, with $\nu, \xi \in (\mathrm{I, II, III, IVa, IVb, V})$, the functions of (5b) have to be introduced instead of those of (5a).

References

[1] H. Hofmann, "Dispersion of planar waveguides for millimeter-wave application," *Arch. Elek. Übertragung.*, vol. 31, pp. 40–44, Jan. 1977.

[2] L. P. Schmidt and T. Itoh, "Spectral domain analysis of dominant and higher order modes in finlines," *IEEE Trans. Microwave Theory Tech.*, vol. MTT-28, pp. 981–985, Sept. 1980.

[3] L. P. Schmidt, T. Itoh, and H. Hofmann, "Characteristics of unilateral fin-line structures with arbitrarily located slots," *IEEE Trans. Microwave Theory Tech.*, vol. MTT-29, pp. 352–355, Apr. 1981.

[4] L. P. Schmidt, "A comprehensive analysis of quasiplanar waveguides for millimeter-wave application," in *11th Eur. Microwave Conf. Proc.* (Amsterdam, Netherlands), Sept. 7–10, 1981, pp. 315–320.

[5] R. N. Simons, "Analysis of millimeter-wave integrated fin line," *Inst. Elec. Eng. Proc., Microwaves, Optics and Antennas*, vol. 130, pt. H., pp. 166–169, Mar. 1983.

[6] A. K. Sharma and W. J. R. Hoefer, "Propagation in coupled unilateral and bilateral finlines," *IEEE Trans. Microwave Theory Tech.*, vol. MTT-31, pp. 498–502, June 1983.

[7] A. Beyer, "Analysis of the characteristics of an earthed fin line," *IEEE Trans. Microwave Theory Tech.*, vol. MTT-29, pp. 676–680, July 1981.

[8] R. Vahldieck, "Accurate hybrid-mode analysis of various finline configurations including multilayered dielectrics, finite metallization thickness, and substrate holding grooves," *IEEE Trans. Microwave Theory Tech.*, vol. MTT-32, pp. 1454–1460, Nov. 1984.

[9] J. Bornemann, "Rigorous field theory analysis of quasi-planar waveguides," *Inst. Elec. Eng.. Proc., Microwaves, Optics and Antennas*, vol. 132, pt. H. pp. 1–6, Feb. 1985.

[10] T. Kitazawa and R. Mittra, "Analysis of finlines with finite metallization thickness," *IEEE Trans. Microwave Theory Tech.*, vol. MTT-32, pp. 1484–1487, Nov. 1984.

[11] F. Arndt and U. Paul, "The reflection definition of the characteristic impedance of microstrips," *IEEE Trans. Microwave Theory Tech.*, vol. MTT-27, pp. 724–731, Aug. 1979.

[12] S.-T. Peng and A. A. Oliner, "Guidance and leakage properties of a class of open dielectric waveguides: Part I—mathematical formulations," *IEEE Trans. Microwave Theory Tech.*, vol. MTT-29, pp. 843–854, Sept. 1981.

[13] R. Sorrentino and T. Itoh, "Transverse resonance analysis of finline discontinuities," *IEEE Trans. Microwave Theory Tech.*, vol. MTT-32, pp. 1633–1638, Dec. 1984.

[14] R. H. Jansen, "Unified user-oriented computation of shielded, covered and open planar microwave and millimeter-wave transmission-line characteristics," *Microwaves, Opt. Acoust.*, vol. 3, pp. 14–22, Jan. 1979.

[15] H. Brandis and W. Schminke, "Zur Definition des Leitungswellenwiderstands der geschirmten Streifenleitung," *Frequenz*, vol. 34, pp. 30–32, Feb. 1980.

[16] R. Sorrentino, G. Leuzzi, and A. Silbermann, "Characteristics of metal–insulator–semiconductor coplanar waveguides for monolithic microwave circuits," *IEEE Trans. Microwave Theory Tech.*, vol. MTT-32, pp. 410–416, Apr. 1984.

[17] R. Vahldieck and J. Bornemann, "A modified mode matching technique and its application to a class of quasi-planar transmission lines," *IEEE Trans. Microwave Theory Tech.*, vol. MTT-33, pp. 916–926, Oct. 1985.

[18] J. P. Villotte, M. Aubourg, and Y. Garault, "Modified suspended striplines for microwave integrated circuits," *Electron. Lett.*, vol. 14, no. 18, pp. 602–603, Aug. 31, 1978.

Jens Bornemann was born in Hamburg, West Germany, on May 26, 1952. He received the Dipl.-Ing. and the Dr.-Ing. degrees in electrical engineering from the University of Bremen, Bremen, West Germany, in 1980 and 1984, respectively.

Since 1980, he has been with the Microwave Department of the University of Bremen, where his current research activities include microwave integrated-circuit filter design, printed E-plane technology for millimeter-wave applications, and problems of electromagnetic field theory, especially those requiring numerical methods of solution.

Dr. Bornemann is one of the recipients of the A. F. Bulgin Premium of the Institution of Electronic and Radio Engineers, 1983.

Fritz Arndt (SM'83) was born in Konstanz, West Germany, on April 30, 1938. He received the Dipl.-Ing. the Dr.-Ing., and the Habilitation degrees from the Technical University of Darmstadt, West Germany, in 1963, 1968, and 1972, respectively.

From 1963 to 1972, he worked on directional coupler and microstrip techniques at the Technical University of Darmstadt. Since 1972, he has been a Professor and Head of the Microwave Department at the University of Bremen, West Germany. His research activities are, at present, in the area of the solution of field problems of waveguide, finline, and optical waveguide structures, of antenna design, and of scattering structures.

Dr. Arndt is member of the VDE and NTG (Germany). In 1970, he received the NTG award, and in 1983 the A. F. Bulgin Award (together with Dr. Bornemann and two coauthors) from the Institution of Radio and Electronic Engineers.